Properties of mixed transition metal oxides: MM'O3 in corundum-type structures (M,M'=Al,Ti,V,Cr,and Fe)

H.-L. Le, Jacek Goniakowski, C. Noguera

Properties of mixed transition metal oxides: $MM'O_3$ in corundum-type structures (M, M' = Al, Ti, V, Cr, and Fe).

H-L.T. Le,[1] J. Goniakowski,[1] and C. Noguera[1]

[1] *CNRS-Sorbonne Université, UMR 7588, INSP, F-75005 Paris, France*

(Dated: July 7, 2018)

The growing interest of modern technologies for oxide materials is in part due to the possibility of their doping and/or mixing, which often leads to artificial compounds with tunable properties, such as, e.g., the gap width or the band edge positions. However, engineering of mixed oxide materials requires a better fundamental understanding of their structural, electronic, and ordering properties, well beyond low doping levels, and with a reference to their parent materials. In the present work, a series of mixed $MM'O_3$ oxides (M, M' = Al, Ti, V, Cr, Fe) in three corundum-type structures: ilmenite, $LiNbO_3$, and C is studied by means of first principles DFT+U simulations. We find that, regardless the precise atomic structure, the local structural and electronic characteristics of most of the compounds are very close to those of their parent corundum M_2O_3 oxides. The two noticeable exceptions are $TiVO_3$ and $TiFeO_3$, for which the structural, electronic, and magnetic characteristics are consistent with a mixing-induced change of the cation oxidation states. We show that this actual oxydo-reduction process can be rationalized by analyzing the relative band edge positions of the parent oxides. The formation energies of these mixed oxides correlate well with the experimental evidence and, within a mean field approximation, allow predicting the thermodynamics of solid solutions $M_{1-x}M'_xO_3$ at finite temperature.

I. INTRODUCTION

Oxides are the most abundant compounds in our natural environment and, since long, have been used in catalysis, electronics, optoelectronics, or as thermal or electrical insulating barriers. Nowadays, modern technologies attempt to fine tune their properties by means of nano-structuration or doping, producing "artificial" oxide compounds of required characteristics, which often have no natural counterparts. For example, doping ZnO by magnetic atoms allowed obtaining magnetic semiconductors[1,2]. Mixing two oxides has often been considered as a way to engineer the band gap, as exemplified by the $Zn_{1-x}Mg_xO$ alloy, which is a transparent material active in the ultraviolet region of the optical spectrum with applications in optoelectronics[3], or by $Ti_{1-x}Sn_xO_2$ alloy[4]. Similarly, doping perovskites (e.g., $BaTiO_3$) with iron enables engineering the band edge positions, which makes these materials useful as anodes in photo-assisted water-electrolysis[5].

The interest in mixed oxide compounds has called for a better understanding of their structural, electronic, and ordering properties, not only at low doping but also in a wider composition range. In the past, several studies of phase diagrams of mixed rocksalt[6,7] or corundum[8] oxides have been performed, based on pair-potential approaches. First principles simulations have been mainly devoted to studies on the dilute limit, where extremely few — often a single — doping cation or anion are introduced in the repetitive unit cell[9–12]. The focus in that case is principally on the local lattice distortions around the impurity, the position of the defect electronic states in the band gap, and the resulting magnetic structure.

The goal of the present study is a first principles analysis of the strong doping limit, which has hardly been tackled in the past[13], especially in the case of multivalent cations, for which changes of the oxidation state with respect to the pure parent compounds may occur. To this goal we have considered a series of corundum $MM'O_3$ transition metal mixed oxides (M, M' = Ti, V, Cr, and Fe), which enables establishing links between the structural, electronic, and energetic characteristics of the mixed compounds and the corresponding parent oxides. The series contains ilmenite $TiFeO_3$, commonly found in metamorphic and igneous rocks[14], but also $TiVO_3$, which does not naturally exist but has been recently synthesized as a supported thin film[15]. As to broaden the perspective over a case of a larger lattice mismatch, larger bond ionicity, and *sp* cation character, we also included the $TiAlO_3$ compound, obtained by mixing corundum Al_2O_3 and Ti_2O_3.

The paper is organized in the following way. After a description of the computational details (Section II), in Section III, we first summarize the reference data obtained for the pure parent M_2O_3 oxides and then present our findings on the structural and electronic properties of $MM'O_3$ in three different bulk atomic structures. A discussion follows (Section IV) highlighting the physical origin of the behavior displayed by these mixed oxides, before a conclusion.

II. COMPUTATIONAL DETAILS

DFT calculations were performed with the Vienna Abinitio Simulation Package (VASP)[16,17] using the Projector Augmented Wave (PAW) method[18,19] to represent the electron-core interaction and a 400 eV energy cutoff in the development of Kohn-Sham orbitals on a plane-wave basis set. Transition metal (TM) $3p$ states were systematically considered as semi-core states. Dispersion-corrected (optB88-vdW)[20–22] exchange-correlation func-

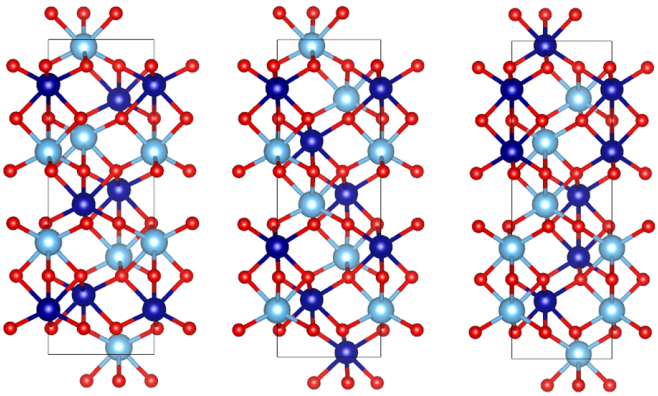

FIG. 1. Bulk unit cells of mixed MM'O_3 oxides in the ilmenite (left), $LiNbO_3$ (middle) and C (right) structures. Cations and anions are represented as large blue (light and dark) and small red balls, respectively.

tional was employed, within the DFT+U approach proposed by Dudarev[23,24]. We have used U values close to those reported in the literature: $U = 1$ eV for Ti_2O_3[25], $U = 1.7$ eV for V_2O_3[26,27], and $U = 3$ eV for Cr_2O_3 and Fe_2O_3[28]. All calculations were spin-polarized and the relative stability of simple non-magnetic (NM), ferro-magnetic (FM), and alternative anti-ferromagnetic (AF) solutions was systematically tested. Ionic charges were estimated with the partition scheme proposed by Bader[29,30] and magnetic moments were obtained by integration of the spin density within the Bader's volumes. Atomic configurations were plotted with VESTA[31].

Compounds of the MM'O_3 stoichiometry may adopt the ilmenite, lithium niobate ($LiNbO_3$) or perovskite structures, depending upon thermodynamic conditions. For example, ilmenite is the most stable $TiFeO_3$ polymorph at ambient pressure and temperature. It transforms into the lithium niobate phase at elevated temperature and into the perovskite phase at high pressures[32]. Targeting principally the ambient pressure conditions, we have focused on mixed MM'O_3 oxides in corundum-type structures and have considered three different cation orderings, Fig. 1. In the ilmenite structure M and M' cations are ordered into pure M or M' layers alternating along the hexagonal c axis, while in the lithium niobate structure they form mixed {M,M'} layers. Moreover, in this latter case, the short cation-cation bond along the c axis may involve either dissimilar (genuine $LiNbO_3$ structure) or similar (structure labeled C in the following) cations. The C structure, characterized by two inequivalent anions, has already been discussed in the case of $MnTiO_3$ compound[33], but, to our knowledge, has not yet been observed experimentally.

An hexagonal corundum unit cell containing six formula units was used in the simulations of all parent and mixed oxides and the sampling of its Brillouin zone was performed with a Γ-centered $(8 \times 8 \times 3)$ Monkhorst-Pack mesh[34].

The formation energy of the mixed compounds with respect to their parent oxides is calculated as:

$$E^{form} = E_{MM'O_3} - \frac{E_{M_2O_3} + E_{M'_2O_3}}{2} \quad (1)$$

where $E_{M_2O_3}$, $E_{M'_2O_3}$ and $E_{MM'O_3}$ are the total energies of one formula unit of bulk M_2O_3, M'$_2O_3$, and MM'O_3, respectively.

III. RESULTS

Before presenting the computational results on the mixed MM'O_3 compounds, we first briefly summarize the reference data on the corresponding pure parent M_2O_3 oxides (Section III A). For the sake of clarity, we then provide a comprehensive description of the mixed compounds in their most stable ilmenite structure (Section III B), before highlighting the principal similarities and differences between the three alternative structures (Section III C).

A. Pure M_2O_3 oxides

The structural (lattice parameters, inter-atomic distances) and electronic properties (charges, band gaps, magnetic moments and structures) of the five corundum parent oxides M_2O_3 (M = Al, Ti, V, Cr, Fe) are summarized in Tab. 1 and their ion-projected densities of states (LDOS) are given in Fig. 2.

TABLE 1. Calculated properties of corundum M_2O_3 oxides (M = Al, Ti, V, Cr, Fe): lattice parameters a and c (Å), cation-oxygen bondlengths d_{M-O} (Å), Bader charges (e) on cations Q_M and anions Q_O, cation magnetic moment μ_M (μ_B), gap G (eV), and ground state magnetic ordering MS (when two labels are given, the first one refers to in-plane coupling, and the second to inter-plane coupling along the short cation-cation bond). Experimental values are recalled in brackets.

	Al_2O_3	Ti_2O_3	V_2O_3	Cr_2O_3	Fe_2O_3
a	4.80	5.14	5.05	5.04	5.06
	(4.75)	(5.16)	(4.99)	(4.96)	(5.04)
c	13.11	13.91	14.12	13.77	13.87
	(12.97)	(13.61)	(13.98)	(13.60)	(13.75)
d_{M-O}	1.87, 1.99	2.03, 2.09	1.99, 2.09	1.99, 2.05	1 .95, 2.13
Q_M	2.48	1.91	1.84	1.76	1.74
Q_O	-1.66	-1.27	-1.23	-1.18	-1.16
G	6.4	0.	0.35	2.76	1.72
	(8.8)	(0.1)	(0.)	(3.4)	(2.2)
μ_M	0.	0.	1.7	2.9	4.0
	(0.)	(0.)	(2)	(3.8)	(4.6-4.9)
MS	NM	NM	(AF,AF)	(AF,AF)	(FM,AF)

In all cases, the overall agreement between the calculated and experimental characteristics is fairly satisfac-

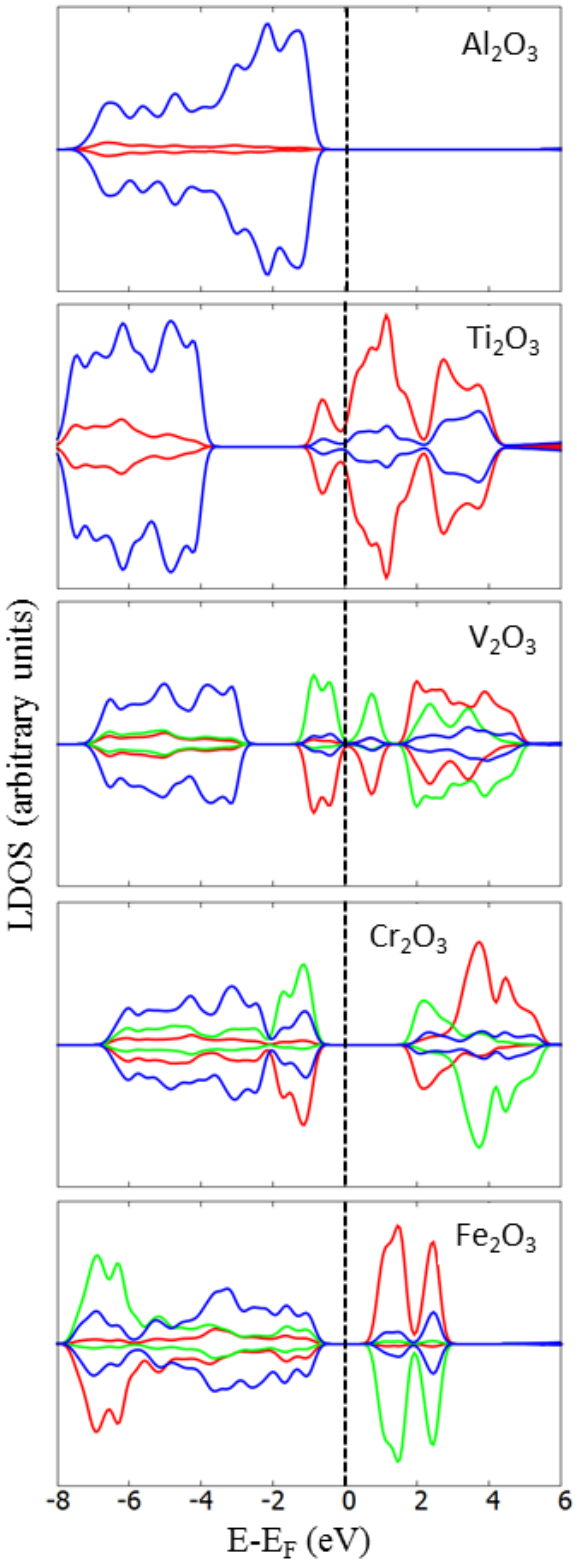

FIG. 2. Projected densities of states in corundum M_2O_3 oxides (M = Al, Ti, V, Cr, Fe) on anions (blue lines) and cations (red lines in non-magnetic Al_2O_3 and Ti_2O_3, red and green lines in anti-ferromagnetic V_2O_3, Cr_2O_3, and Fe_2O_3). Black dashed lines indicate the position of the Fermi level.

tory. In particular, the calculated lattice parameters of all oxides differ by less than 2% from the experimental ones[35,36]. Al_2O_3 is correctly found as a non-magnetic charge-transfer insulator, with the top of the valence band (VBM) essentially made of oxygen states, and the bottom of the conduction band (CBm) made of aluminum states, but its gap suffers from the usual DFT underestimation. Cr_2O_3 and Fe_2O_3 are correctly found as anti-ferromagnetic semiconductors, with a mixed charge-transfer-Mott-Hubbard character[37]. The states at the top of their VB have an hybridized oxygen-cation character (stronger in Fe_2O_3), while the bottoms of their CB are mostly cationic. Thanks to the DFT+U correction, their gaps are only little underestimated. The cation magnetic moments reveal a high spin state (three and five d electrons, respectively), corresponding to the formal oxidation state +3. Their spin orderings are in agreement with experiment, i.e. G-type AFM for Cr_2O_3 [(AF,AF) in Tab. 1] and C-type AFM for Fe_2O_3 [(FM,AF)].

Ti_2O_3 is a spin-paired metal at high temperature and displays a transition (MI) towards a Mott-Hubbard semiconducting state around 470 K, without modification of its rhombohedral structure and without apparition of long range magnetic order[37,38]. In its low temperature phase, the opening of a small gap (0.1 eV) is assigned to the formation of Ti-Ti pairs along the short bond parallel to the c axis, which shifts the bonding a_g state below the conduction band. Our calculated non-magnetic metallic structure of Ti_2O_3 is fully consistent with this picture. There exists a filled Ti a_g bonding state just below the Fermi level, consistent with the Ti +3 oxidation state. However, since the calculated Ti-Ti distance (2.63 Å) is slightly larger than the experimental one at low temperature (2.58 Å[36]), the a_g bonding-antibonding gap is slightly too small in our simulation.

V_2O_3 has a paramagnetic metallic phase at high temperature and displays a MI transition of the Peierls-Mott type at 150 K towards a monoclinic anti-ferromagnetic Mott-Hubbard insulating state with an optical gap of 0.5-0.6 eV[37]. Polarization-dependent x-ray absorption measurements[39] indicate that the spin is S=1 in both phases. Consistently with experiments, and despite the imposed corundum structure, we find a G-type anti-ferromagnetic semi-conducting ground state. The two V filled states below the Fermi level are consistent with the +3 oxidation state of vanadium.

In summary, despite the approximate character of the DFT+U approach, the present results account correctly for both the structural and electronic characteristics of the M_2O_3 oxides under consideration. Importantly, while the band gaps suffer from some underestimations, the calculations reproduce satisfactorily the character of the electronic structure in the Fermi level vicinity as well as the experimental magnetic orderings.

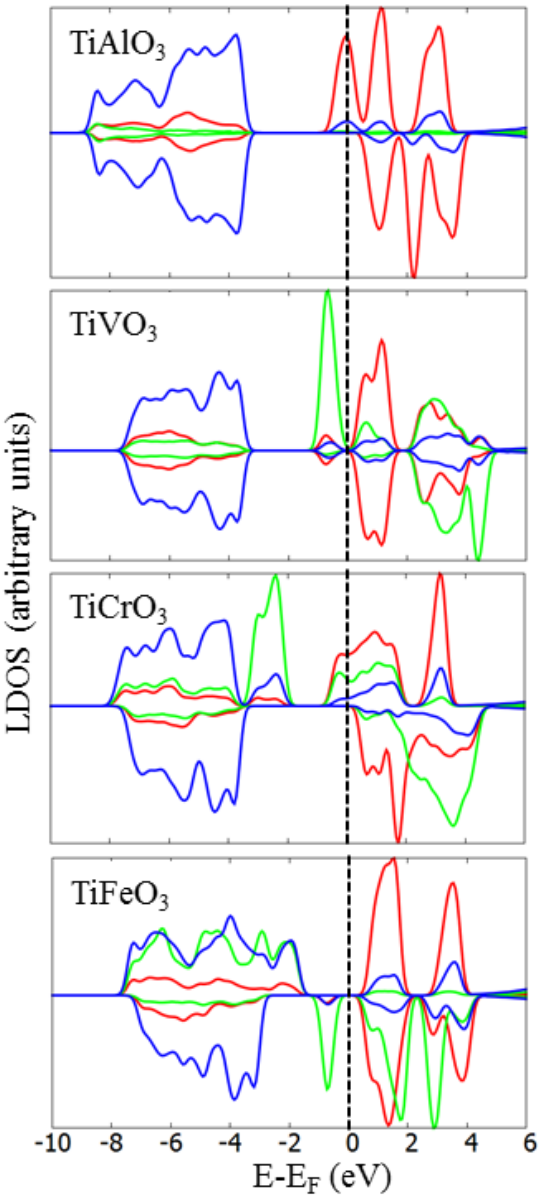

FIG. 3. $MM'O_3$ ($TiAlO_3$, $TiVO_3$, $TiCrO_3$ and $TiFeO_3$) density of states, projected on cations (red and green lines for M and M', respectively) and oxygen atoms (blue lines) in the ilmenite bulk structure. Black dashed lines indicate the position of the Fermi level.

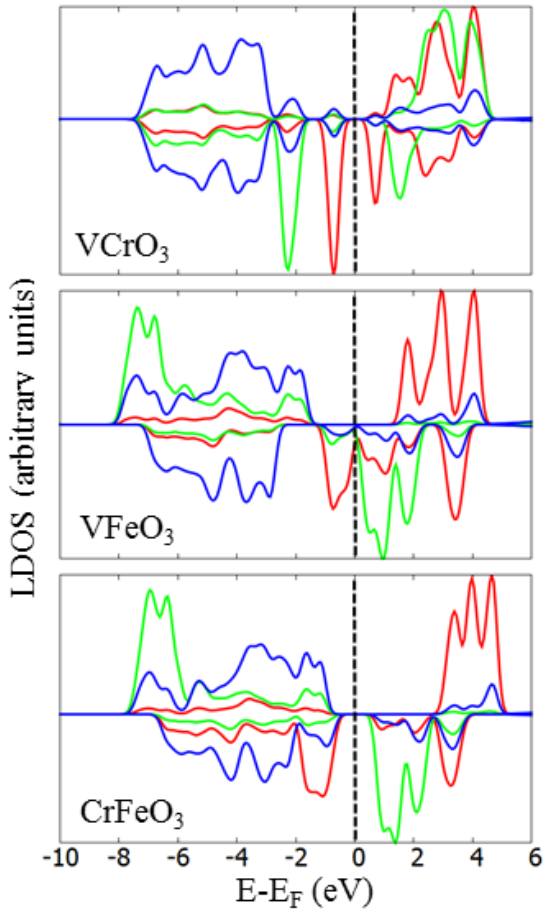

FIG. 4. Same as Fig. 3 for $VCrO_3$, $VFeO_3$ and $CrFeO_3$.

B. Mixed $MM'O_3$ compounds: Ilmenite structure

Table 2 summarizes the structural, electronic, magnetic, and energetic properties of the series of mixed transition metal oxides in the ilmenite structure. Their projected densities of states are displayed in Figs. 3 and 4. In the following we will systematically refer to M and M' as the first and the second cation in the $MM'O_3$ formula, respectively.

Based on these results, the mixed compounds can be split into two groups, depending on how much their structural and electronic characteristics differ from those of their parent materials. While in most cases the mixing induces relatively small modifications, $TiVO_3$ and $TiFeO_3$ stand out by a substantial change of their local properties. We will see in the following that their structural and electronic characteristics concomitantly provide a clear evidence of a change of cation oxidation states.

From the structural point of view, mixed oxides experience small elastic distortions with respect to their parents. The largest relative difference of lattice parameters a and c is equal to 7% between Al_2O_3 and Ti_2O_3, but does not exceed 2% between the transition metal oxides. We note that, while the inter-atomic distances d_{M-O} and $d_{M'-O}$ remain close to their parent values in most $MM'O_3$ mixed compounds, d_{Ti-O} exhibit a noticeable decrease and $d_{M'-O}$ (M'=V, Fe) a noticeable increase in $TiVO_3$ and $TiFeO_3$. According to the behavior of cation ionic radii:[40] $r_{M^{4+}} < r_{M^{3+}} < r_{M^{2+}}$, such structural modification upon mixing is consistent with an increase of the Ti oxidation state and its decrease for V and Fe. It is further confirmed by a comparison with inter-atomic distances in TiO_2, VO and FeO (Tab. 5 in the appendix).

TABLE 2. Properties of mixed MM'O_3 compounds in the ilmenite structure (M, M' = Al, Ti, V, Cr, Fe): lattice parameters a and c (Å), Bader charges (e) on cations Q_M, $Q_{M'}$ and anions Q_O, gap G (eV), magnetic moments μ_M, $\mu_{M'}$ (μ_B), magnetic ordering MS (the three shortest distance magnetic couplings are given: in-plane, inter-plane along the short cation-cation bond, and inter-plane between second neighbors), and formation energy E^{form} (eV/formula unit) with respect to pure corundum parents.

Ilmenite	$TiAlO_3$	$TiVO_3$	$TiCrO_3$	$TiFeO_3$	$VCrO_3$	$VFeO_3$	$CrFeO_3$
a	4.94	5.11	5.10	5.16	5.03	5.06	5.07
c	13.88	14.11	14.12	13.92	14.01	13.93	13.74
d_{M-O}	2.03, 2.12	1.93, 2.11	1.96, 2.13	1.91, 2.10	1.99, 2.09	1.97, 2.06	1.99, 2.02
$d_{M'-O}$	1.87, 2.00	2.10, 2.11	2.04, 2.10	2.08, 2.20	1.99, 2.05	1.97, 2.17	1.96, 2.17
Q_M	1.93	2.10	2.03	2.16	1.86	1.90	1.78
$Q_{M'}$	2.48	1.61	1.65	1.46	1.75	1.69	1.74
Q_O	-1.47	-1.24	-1.24	-1.20	-1.20	-1.20	-1.17
G	0.0	0.5	0.0	1.0	1.2	0.1	1.4
μ_M	0.9	0.0	0.6	0.1	1.7	1.6	2.8
$\mu_{M'}$	0.0	2.3	3.3	3.7	2.9	4.0	4.1
MS	(FM,-,-)	(AF,-,-)	(FM,FM,FM)	(FM,-,-)	(AF,FM,AF)	(FM,AF,AF)	(FM,AF,AF)
E^{form}	+0.29	-0.35	+0.044	-0.79	0.00	-0.10	+0.08
Config	$Ti^{3+}Al^{3+}$	$Ti^{4+}V^{2+}$	$Ti^{3+}Cr^{3+}$	$Ti^{4+}Fe^{2+}$	$V^{3+}Cr^{3+}$	$V^{3+}Fe^{3+}$	$Cr^{3+}Fe^{3+}$

From the electronic point of view, Bader oxygen charges Q_O(MM'O_3) are systematically very close to the average of their parent oxides (Q_O(M_2O_3) + Q_O(M'$_2O_3$))/2. Since in the ilmenite structure each oxygen is bound to three M and three M' cations, this may suggest that there is a negligible change of iono-covalent character of the cation-oxygen bonds upon formation of the mixed oxide. However, while consistently with this picture, the Bader charges of cations Q_M, $Q_{M'}$ change little with respect to their parents in most of the mixed compounds, this is not the case for $TiVO_3$ or $TiFeO_3$ in which a noticeable increase of the Ti charge and a decrease of the Fe and V ones take place. Although the Bader charges cannot straightforwardly give information on the formal charges, the large δQ_M values corroborate the change of the oxidation states in these two oxides. As a consequence, the relationship Q_O(MM'O_3)$\sim$ (Q_O(M_2O_3)+Q_O(M'$_2O_3$))/2 in $TiVO_3$ and $TiFeO_3$ does not indicate a negligible change of iono-covalent character of the cation-oxygen bonds but rather results from a compensation between those of Ti-O and M'-O bonds.

Also the values of the cation magnetic moments are consistent with the distinct character of these two materials. Indeed, in $VCrO_3$, $VFeO_3$, and $CrFeO_3$, μ_M and $\mu_{M'}$ differ little from those in the parent oxides. In $TiCrO_3$ and $TiAlO_3$, the Ti magnetic moment of the order of 1 μ_B is consistent with the presence of a single electron (Ti +3 state) and the absence of the Ti-Ti paring which exists in Ti_2O_3. Tab. 2 indicates the nature of the in-plane and inter-plane magnetic couplings. The in-plane Ti-Ti, Cr-Cr (except in $VCrO_3$) and Fe-Fe magnetic coupling is ferromagnetic and the V-V one is anti-ferromagnetic, similarly to those in the parent oxides for V, Fe, and Cr in the case of $VCrO_3$. Inter-plane V-Fe, Cr-Fe and V-Cr are anti-ferromagnetic while the Ti-Cr one is ferromagnetic, similar to the V-Cr along the short bond parallel to the c axis. At variance, in $TiVO_3$ and $TiFeO_3$, the Ti magnetic moments are close to zero and the magnetic moments of V and Fe are significantly changed compared to those in V_2O_3 and Fe_2O_3, congruent with an electron transfer from Ti towards V and Fe in these two compounds. The vanadium magnetic moment has increased by nearly one Bohr magneton, as expected from the addition of one electron in this strong Mott-Hubbard oxide. The change in iron magnetic moment is smaller but its similarity with the value obtained in rocksalt FeO within the same simulation set-up points towards an actual Fe^{2+} state (see also Tab. 5 in the appendix). Due to the odd number of Fe layers in our simulation cell, we were not able to reproduce the full $TiFeO_3$ magnetic structure with alternating positive and negative magnetic moments in the Fe layers, as experimentally determined in Reference 41. However, the ferromagnetic in-plane order is well reproduced.

The scenario deduced from the changes of atomic structure, ionic charges, and cation magnetic moments is further validated by the LDOS characteristics, Figs. 3 and 4. Indeed, in $VCrO_3$ and $VFeO_3$ the cation projected DOS are close to those of their parent materials and in $CrFeO_3$ it is nearly a rigid superposition of those of Cr_2O_3 and Fe_2O_3. In $TiAlO_3$, a well-defined isolated Ti majority spin peak exists below Fermi level filled by an unpaired electron (Ti +3 state). An analogous Ti peak can also be identified just below E_F in $TiCrO_3$, where however it is strongly hybridized with Cr states. At variance, the LDOS of $TiVO_3$ and $TiFeO_3$ are substantially modified with respect to their parent oxides. The most important change concerns the Ti-projected DOS, in which the peak located just below E_F in Ti_2O_3 is shifted above the Fermi level and depopulated, thus indicating a change from 3+ to 4+ oxidation state. Si-

multaneously, the weight of V and Fe states just below E_F is enhanced, consistent with a change from 3+ to 2+ oxidation state. We note that the present assignment of Ti^{4+} and Fe^{2+} oxidation states in $TiFeO_3$ is in agreement with a previous simulation of ilmenite[42].

As far as formation energies are concerned, Tab. 2, three qualitatively different behaviors can be defined: E^{form} is large and positive in $TiAlO_3$, large and negative in $TiVO_3$ and $TiFeO_3$, and small (positive or negative) in the remaining mixed oxides. The large and positive E^{form} of $TiAlO_3$ is likely driven by the large lattice misfit and the large difference of bond iono-covalency between Al_2O_3 and Ti_2O_3. At variance, the two mixed transition metal oxides for which the change of the cation oxidation state takes place are characterized by strongly negative mixing energies.

Before concluding this description, let us stress two more points. First, $TiVO_3$ and $TiFeO_3$ display large and negative formation energies not only with respect to their M_2O_3 parent oxides, but also with respect to the TiO_2 and VO or FeO oxides (-0.49 and -0.20 eV per formula unit, respectively, TiO_2, VO and FeO being simulated in their rutile and rocksalt structures). Second, ilmenite $TiFeO_3$ indeed exists as a naturally occurring mineral, at the origin of the generic name 'ilmenite' given to ternary oxides which crystallize in its structure. To our knowledge, the naturally existing mixed Ti-V oxide is Berdesinskiite TiV_2O_5 (Ti and V in +4 and +3 oxidation states, respectively)[35] rather than $TiVO_3$, but a corundum-structured thin film of $TiVO_3$ has recently been synthesized on c-cut sapphire[15], for which a strong contribution of Ti^{4+} was evidenced by X-ray photo-electron spectroscopy. Finally, vanadomagnetite V-Fe oxide compounds exist, but only at small vanadium concentrations. The most stable ordered ternary mineral containing these two cations is Coulsonite FeV_2O_4 in which Fe and V are in +2 and +3 oxidation states, respectively[35].

In summary, despite the arbitrary character of the projection scheme employed in the evaluation of atomic charges, magnetic moments, and LDOS, our computational results clearly reveal a different behavior of $TiVO_3$ and $TiFeO_3$ as compared to the other mixed compounds upon consideration. Indeed, while in most cases the changes induced by mixing are small or even negligible, the local structural, electronic, and magnetic characteristics of these two compounds differ substantially from those of their parent oxides. The mixing-induced modifications concomitantly point towards an increase of the Ti oxidation state (3+→ 4+) and a simultaneous decrease of those of V and Fe (3+→ 2+). This sound modification of the electronic structure correlates with a pronounced tendency for mixing (large negative E^{form}), and is consistent with the experimental evidence.

C. Mixed $MM'O_3$ compounds: $LiNbO_3$ and C structures

The structural, electronic, and magnetic characteristics of the mixed oxides in the two alternative $LiNbO_3$ and C-structures are systematically very close to those reported for the ilmenite structure. The full results are thus moved to the Appendix, Tabs. 6 and 7, while, in the following, we restrict the presentation to the most pronounced differences and focus more particularly on the formation energetics.

Indeed, compared to ilmenite, from a structural point of view, in most compounds, the lattice parameters a and c of the three structures differ by less than 0.02 Å and 0.1 Å, which corresponds to relative differences of less than 1% and 2%, respectively, and all cation-oxygen distances d_{M-O} and $d_{M'-O}$ differ by less than 0.05 Å only. Similarly, the electronic characteristics are very similar — the anion and cation charges and the cation magnetic moments are nearly identical (to within 0.02 e and less than 0.1 μ_B), and the LDOS in the vicinity of the Fermi level are practically the same. Consequently, the mixing-induced changes of the cation oxidation states reported for $TiVO_3$ and $TiFeO_3$ in the ilmenite structure also take place for these two compounds in the $LiNbO_3$ and C structures.

The unique noticeable dissimilarity between the three structures concerns $TiCrO_3$, for which $\delta c = 0.25$ Å (relative difference of 2%), $\delta Q_{Cr} = 0.08$ e and $\delta\mu_{Cr} = 0.6$ μ_B. The characteristics of the mixed compound in the $LiNbO_3$ and C structures are visibly closer to those of the parent Cr_2O_3 and Ti_2O_3, while the ilmenite structure is characterized by a more pronounced modification. By inspecting the projected densities of states of $TiCrO_3$ in the three structures, Fig. 5, this difference can be assigned to a more pronounced hybridization between Cr and Ti in the peak just below Fermi level.

As far as the relative stability of the three structures is concerned, Tab. 3 shows that the specificities of formation energies reported for the ilmenite structure are preserved: E^{form} are large and positive for $TiAlO_3$, large and negative for $TiVO_3$ and $TiFeO_3$ and smaller (either positive or negative) for all other mixed oxides. Ilmenite is the most stable polymorph, characterized by the most negative or the smallest positive formation energies. $CrFeO_3$ constitutes the unique exception, with the $LiNbO_3$ structure being the most stable. We note however that energy differences between the two most stable structures may be as small as 0.02 eV per formula units ($TiVO_3$, $VCrO_3$, $CrFeO_3$), likely close to the precision of the present estimation. Similarly, the $LiNbO_3$ structure is more stable than the C structure in all mixed transition metal oxides. The reverse is true in $TiAlO_3$ only, where the formation of short Ti-Ti bonds along the c-axis enables a small energy gain.

Despite small differences between the various polymorphs, the formation energies of the mixed oxides follow a general trend. In the case of $TiVO_3$ and $TiFeO_3$,

TABLE 3. Formation energies E^{form} (eV per formula unit) of mixed MM'O_3 compounds in the ilmenite, $LiNbO_3$, and C structures together with the deduced values of effective cation-cation mixing parameters W_1, W_2 and W_3 (see text) (eV).

	$TiFeO_3$	$TiVO_3$	$VFeO_3$	$VCrO_3$	$TiCrO_3$	$CrFeO_3$	$TiAlO_3$
Ilmenite	-0.79	-0.35	-0.10	0.00	0.04	0.08	0.29
$LiNbO_3$	-0.73	-0.33	-0.01	0.02	0.16	0.06	0.60
C	-0.56	-0.28	0.01	0.04	0.19	0.15	0.40
W_1	-0.083	-0.0433	0.0167	0.01	0.0517	0.0217	0.1183
W_2	-0.3247	-0.125	-0.0397	-0.0153	-0.0125	-0.0478	0.2225
W_3	-0.0517	-0.025	-0.0067	0.0017	0.00583	0.0142	0.0075

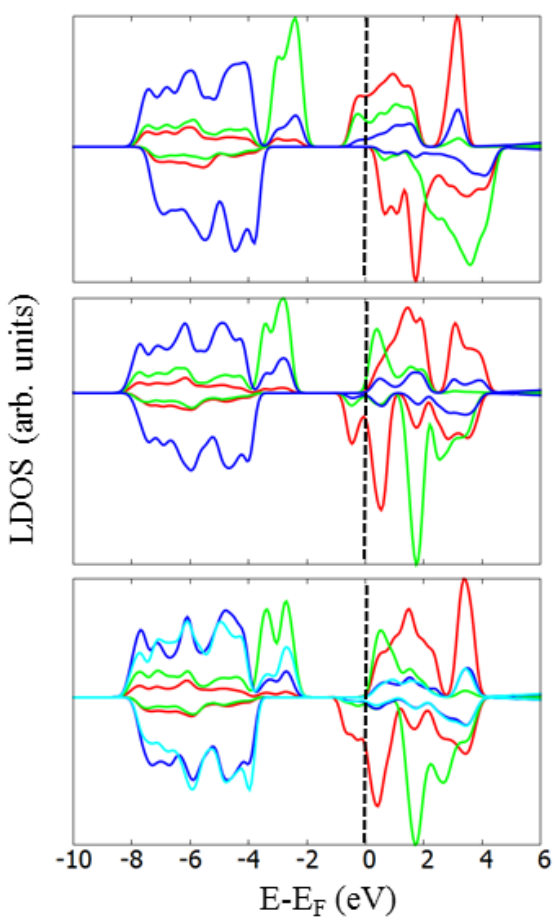

FIG. 5. Projected densities of states of $TiCrO_3$ [Ti (red), Cr (green), and O (blue and cyan)] in the ilmenite (left), $LiNbO_3$ (middle), and C (right) structures.

in which a redox reaction takes place, the large negative mixing energy is mainly driven by the gain of band energy, associated with electron transfers from Ti states (higher on the energy scale) towards V and Fe states (lower on the energy scale) and the associated gain of electrostatic energy. In other mixed transition metal oxides, in the absence of such a strong stabilizing effect, the formation energies are much smaller (in absolute values) and mostly positive as a result of the necessary adjustments of the atomic structure with respect to the local environments in the parent oxides, but also due to the incompatibilities between the parent magnetic structures. In $TiAlO_3$, a system in which no redox reaction takes place, the large difference in cation ionic radii between Ti^{3+} and Al^{3+} induces strong structural distortions upon mixing, leading to a large positive mixing energy.

Formation energies of the three structures enable an estimation of effective short-range in-plane and inter-plane cation-cation interactions. The shortest in-plane cation-cation distance d_1 is of the order of 3 Å (three neighbors), and is much smaller than the second-neighbor one (≈ 5 Å). The shortest inter-plane distance d_2 is of the order of 2.8-2.9 Å (a single neighbor). It is followed by second-neighbor inter-plane distances d_3 in the range 3.4-3.7 Å (nine neighbors). By introducing effective mixing parameters $W_i = 2V_i^{MM'} - V_i^{MM} - V_i^{M'M'}$ associated to interaction energies V_i between cation pairs at distances d_i, it is possible to write the formation energies of the three structures as:

$$\begin{aligned} E_{ilm}^{form} &= W_2 + 9W_3 \\ E_{LNO}^{form} &= 3W_1 + W_2 + 3W_3 \\ E_C^{form} &= 3W_1 + 6W_3 \end{aligned} \quad (2)$$

The values of W_i deduced from the DFT formation energies of the mixed compounds are given in Tab. 3. Positive values of W correspond to preferential formation of pure M-M and M'-M' bonds and thus to a tendency for phase separation, while negative W favor mixed M-M' bonds and thus a tendency for mixing.

Let us first note that the three parameters W_i display a similar behavior along the considered series. They increase progressively from more negative ($TiFeO_3$), through close to zero ($VCrO_3$), up to large positive ($TiAl_3$) values. This behavior parallels that of E^{form} and shows that the latter is due to a concomitant effect of the first, second, and third neighbor cation-cation interactions, rather than a competition between them. Indeed, if W_2 tends to be in most cases somewhat more negative than W_1 and W_3, its overall effect remains small because it concerns a single cation-cation pair.

Conversely, parameters W_1 and W_3 play the major role in the overall energetics due to the large number of cation-cation neighbors they are associated with. Indeed, both parameters are negative for $TiFeO_3$ and $TiVO_3$

(large negative E^{form}), and positive for $VCrO_3$, $TiCrO_3$ and $CrFeO_3$ (positive E^{form}), with values which increase progressively along the series. $TiAlO_3$ behavior is somewhat different. It is the only case in which a large and positive W_2 is met. Since W_3 is nearly vanishing, those are the values of W_1 and W_2 which explain the large positive E^{form} value.

Finally, if the ilmenite structure is favored in all cases but $CrFeO_3$, this preference is relatively small and cannot be easily assigned to a cation-cation interaction between a precise pair of neighbors, but results rather from a complex interplay between in-plane W_1 and out-of-plane W_3 interactions. In this context, one could note that the W_i decrease relatively slowly as a function of cation-cation distance d_i. This is particularly clear when comparing W_1 ($d_1 \approx 3$ Å) and W_3 ($d_3 \approx 3.4$ - 3.7 Å) and may suggest that taking into account effective interactions between more distant cation-cation pairs could yield a finer description of the mixing energetics.

In summary, the structural and electronic characteristics found for the mixed oxides in the ilmenite structure are preserved in the alternative $LiNbO_3$ and C ones. Due to the large number of corresponding cation-cation pairs, the oxide mixing characteristics are driven by concomitant effect of in-plane W_1 and inter-plane W_3 effective cation-cation interactions. If ilmenite structure is favored in most cases, this preference cannot be assigned to the interaction between a specific pair of neighbors. This is partially due to a relatively slow decrease of cation-cation interaction strength as a function of distance. Finally, the decomposition into pair interactions reveals a different nature of interactions in $TiAlO_3$, in which all cation-cation pairs contribute to the particularly strong preference for phase separation.

IV. DISCUSSION

In this last section, we discuss the microscopic mechanisms behind the electronic structure characteristics of mixed compounds and analyze how they can be predicted from those of the parent materials. Furthermore, relying on the mixing energies E^{form} and parameters W_i, we sketch the expected behavior of mixed oxides at finite temperatures and for compositions different from 1/2.

1. *Change of oxidation states*

The analysis of the electronic structure (Section III) has highlighted the existence of strong cation-to-cation electron transfers in some mixed oxides ($TiVO_3$ and $TiFeO_3$) and its absence in the other compounds. The fact that this result does not depend on the precise ordered structure suggests that it is due to intrinsic properties of the parent oxides and that it can be rationalized by general arguments similar to those used, for example, at semiconductor interfaces.

TABLE 4. Values of the parameters Δ_1, Δ_2, and Δ_{BE} (eV) deduced from the band structures of the parent oxides M_2O_3 and M'_2O_3, after the alignment of their oxygen 1s levels, Fig. 6.

M_2O_3-M'_2O_3	Δ_1 (eV)	Δ_2 (eV)	Δ_{BE} (eV)
Ti_2O_3-Fe_2O_3	-1.1	2.8	2.8
Ti_2O_3-V_2O_3	-1.1	1.5	1.5
Ti_2O_3-Cr_2O_3	-0.2	2.9	2.9
V_2O_3-Fe_2O_3	0.4	1.7	1.4
V_2O_3-Cr_2O_3	1.3	1.8	1.5
Cr_2O_3-Fe_2O_3	1.6	2.7	-0.1
Ti_2O_3-Al_2O_3	2.4	4.1	4.1

Electron transfers at semiconductor interfaces have been rationalized in the past by aligning the electronic structures of the two parent materials (their bulks or their surfaces) with respect to a common reference energy which, depending on the authors, was the vacuum level in the "electron affinity rule" model[43], the mean electrostatic potential[44,45], the valence band positions[46], the core level positions[47], the point of zero charge[48–50], or the oxygen 2p states at perovskite-perovskite interfaces[51].

As in this last case, in the mixed corundum $MM'O_3$ compounds the oxygen sub-lattice is shared. We have thus performed an alignment of the oxygen 1s states (estimated by the electrostatic potential at the ionic cores) of the two parent M_2O_3 and M'_2O_3 oxides and have quantified their band-offsets with two parameters Δ_1 =$E_{CBm}(M'_2O_3)$ - $E_{VBM}(M_2O_3)$ and Δ_2 =$E_{CBm}(M_2O_3)$ - $E_{VBM}(M'_2O_3$, Fig. 6 and Tab. 4. Within this definition, negative values of Δ_1 and Δ_2 indicate an overlap between VB and CB of the parent materials, consistent with an electron transfer M→M' and M'→M, respectively.

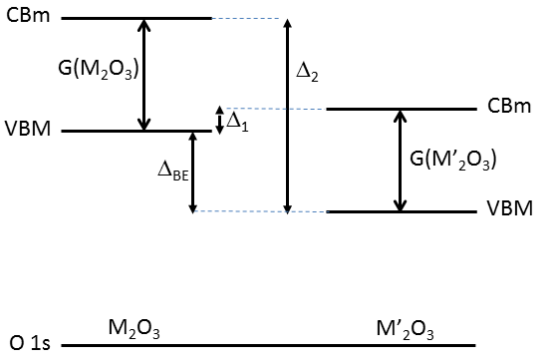

FIG. 6. Relative positions of the valence band maximum (VBM) and conduction band minimum (CBm) of two parent oxides after alignment of their oxygen 1s levels. Parameters Δ_1, Δ_2, and Δ_{BE} (see text) are indicated.

We first notice that, in all cases, the Δ_2 values are large and positive. They show the absence of any overlap between the CB of M_2O_3 and the VB of M'_2O_3, and

the resulting impossibility of an M'→M electron transfer. Indeed, no such transfers have been found in our mixed oxide simulations. Conversely, while Δ_1 is large and positive for Cr_2O_3-Fe_2O_3, V_2O_3-Cr_2O_3 and Ti_2O_3-Al_2O_3 (absence of M→M' electron transfer) it becomes large and negative for Ti_2O_3-Fe_2O_3 and Ti_2O_3-V_2O_3, thus suggesting a possibility of an M→M' electron transfer in these two cases. These predictions clearly match the results of the full calculations on the corresponding mixed oxides. Finally, in the case of V_2O_3-Fe_2O_3 and Ti_2O_3-Cr_2O_3, the absolute values of Δ_1 are much smaller. While for the former, $\Delta_1 > 0$ is consistent with the calculated absence of charge transfer in $VFeO_3$, the negative $\Delta_1 < 0$ for the latter is not consistent with the full calculation results on $TiCrO_3$. However, we stress that the band alignment of the parent materials only determines the initial state for an electron exchange and neglects all the subsequent exchange-induced processes. Such initial state approximation may be questionable whenever the $\Delta_i \sim 0$, as illustrated by the present case of Ti_2O_3-Cr_2O_3.

As to further validate our results in $VFeO_3$ and $TiCrO_3$, we have checked to what extent they are sensitive to the values of U_{Fe} and U_{Cr} used in the DFT+U approach. Fig. 7 shows that, despite substantial variations of the Fe_2O_3 and Cr_2O_3 gap widths, there is no change of sign of Δ_1 when U varies in a wide range 1 eV $< U <$6 eV. Interestingly, the formation energies of these two oxides also keep a constant sign.

In order to give a rationale for the values and trends of Δ_1 and Δ_2, let us note that they involve only the difference of oxygen binding energies (BE) Δ_{BE} = $E_{VBM}(M_2O_3)$ - $E_{VBM}(M'_2O_3)$ and the gap widths $G(M_2O_3)$ and $G(M'_2O_3)$ of the two parent materials, Fig. 6:

$$\begin{aligned} \Delta_1 &= -\Delta_{BE} + G(M'_2O_3) \\ \Delta_2 &= +\Delta_{BE} + G(M_2O_3) \end{aligned} \qquad (3)$$

Using these expressions, the systematically positive values of Δ_2 can be explained by values of Δ_{BE} being systematically larger than (or close to) zero for all the couples of parent materials. The positive binding energy differences Δ_{BE} reflect the progressive decrease of the oxygen 1s BE along the series of the transition metal oxides M_2O_3 (M = Ti, V, Cr, Fe). The negative Δ_1 are driven by large binding energies differences $\Delta_{BE} > G(M'_2O_3)$ found for Ti_2O_3-Fe_2O_3, Ti_2O_3-V_2O_3, and Ti_2O_3-Cr_2O_3. Conversely, positive Δ_1 correspond to cases of smaller Δ_{BE} or larger gap of the parent M'_2O_3, such that $\Delta_{BE} < G(M'_2O_3)$. The cases of Cr_2O_3-Fe_2O_3 (Δ_{BE} = -0.1 eV) and Ti_2O_3-Al_2O_3 [$G(Al_2O_3$ = 6.4 eV $> \Delta_{BE}$] illustrate these two behaviors.

Beyond the mere existence of a cation-to-cation electron transfer, its large value deserves comments and can be related to the Mott-Hubbard character of Ti_2O_3, V_2O_3 and to a lesser extent Fe_2O_3. Indeed, in wide band semiconductors (typically of the *sp* type), a band overlap ΔE induces a small electron transfer due to the low

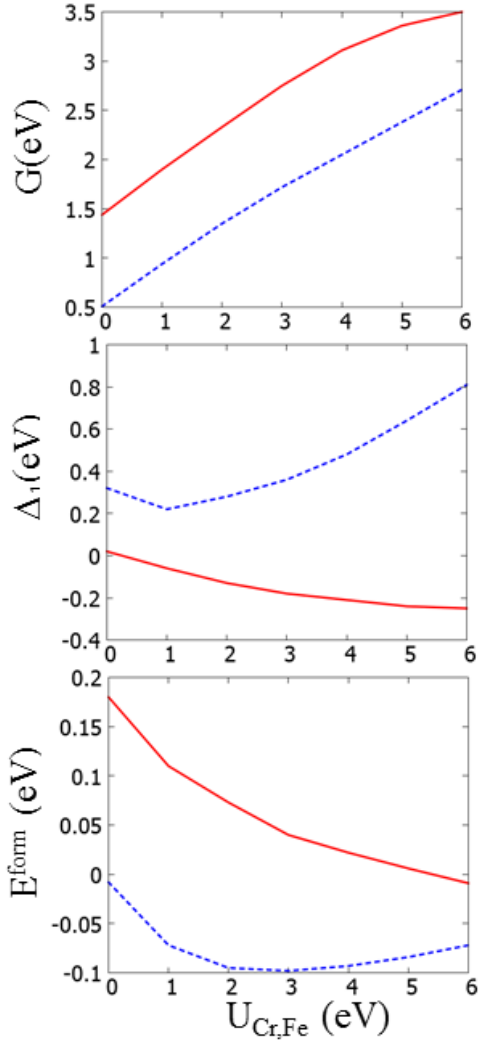

FIG. 7. Calculated band gaps of the parent materials G (eV) (top), Δ_1 (eV) (middle), and formation energies E^{form}(eV) (bottom) for Ti_2O_3-Cr_2O_3 (full red) and V_2O_3-Fe_2O_3 (dashed blue) systems as a function of $U_{Cr,Fe}$ (eV).

density of states at the gap edges. This is not the case in the oxides upon consideration. The states at the gap edges are narrow *d* states, highly localized on cations and associated to a high density of states. A band overlap thus easily induces correlated shifts of whole *d* states across the Fermi level and their associated population and depopulation by one electron. In that case, an actual oxydo-reduction process takes place and it is legitimate to talk of a change of the cation oxidation states.

Finally, let us note that Δ_1 =$E_{CBm}(M'_2O_3)$ - $E_{VBM}(M_2O_3)$ can also provide an estimation of the band gap in the mixed compounds in which no change of oxidation state takes place. Indeed, we find that Δ_1 for $TiCrO_3$, $VFeO_3$, $VCrO_3$ and $CrFeO_3$ (-0.2, 0.4, 1.3 and 1.6 eV, respectively, Tab. 4) correlate well with the calculated values of gaps (0.0, 0.1, 1.2 and 1.4 eV, respectively, Tab. 2), consistently with an M character of their

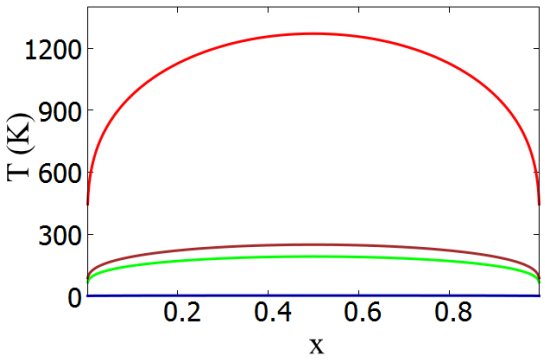

FIG. 8. Estimated miscibility gaps for the $M_{2-2x}M'_{2x}O_3$ solid solutions of mixed oxides with no tendency for mixing ($E^{form} > 0$): $VCrO_3$ (blue), $TiCrO_3$ (green), $CrFeO_3$ (brown), and $TiAlO_3$ (red).

VBM and an M' character of their CBm. In the case of $TiAlO_3$, for which both the VBM and CMm display an Ti character, the zero gap is reminiscent of that in Ti_2O_3.

A. Thermodynamics of mixing

The formation energies that we have calculated characterize the stability of mixed $M_{2-2x}M'_{2x}O_3$ oxides at $T = 0$ K and for equal M and M' concentrations ($x = 1/2$). However a qualitative discussion of their thermodynamics at finite temperatures and in a wider range of composition is possible.

In the case of $Ti_{2-2x}V_{2x}O_3$ and $Ti_{2-2x}Fe_{2x}O_3$, it has been found at $x = 1/2$ that *all* cations experience a change of oxidation state. At compositions $x \neq 1/2$, such a global change will not be possible and Ti^{4+} and Ti^{3+} cations, as well as M'^{2+} and M'^{3+} cations (M' = V or Fe) will coexist. Taking into account the large negative ilmenite $TiVO_3$ and $TiFeO_3$ formation energies, this will very likely lead to a phase separation between $Ti^{4+}V^{2+}O_3$ and $Ti^{3+}V^{3+}O_3$ and between $Ti^{4+}Fe^{2+}O_3$ and $Ti^{3+}Fe^{3+}O_3$.

Ordered $MM'O_3$ mixed oxides with positive formation energies ($VCrO_3$, $TiCrO_3$, $CrFeO_3$, and $TiAlO_3$) are not stable at zero temperature, but they may be stabilized at finite temperatures as disordered (substitutional) solid solutions thanks to disorder effects. Retaining only the entropy contribution of configurational disorder in the Gibbs free energy of formation, the latter reads:

$$G^{form} = E^{form} - 4k_BT\ln 2 \qquad (4)$$

for a $x = 1/2$ solid solution (k_B is the Boltzmann constant). G^{form} becomes negative when $T > T_{max} = E^{form}/(4k_B \ln 2)$. Based on the calculated values of E^{form}, T_{max} is equal to 3, 200, 250, 1300 K, for $VCrO_3$, $TiCrO_3$, $CrFeO_3$, and $TiAlO_3$, respectively. Solid solutions of these mixed oxides at $x = 1/2$ can thus be stable above T_{max}.

Moreover, for the same family of mixed oxides within a mean field approach, one can use the zero of the Gibbs free energy :

$$G^{form} = 4x(1-x)E^{form} - 4k_BT(x\ln x + (1-x)\ln(1-x)) \qquad (5)$$

to estimate above which temperature T a solid solution of composition x can be stable. Figure 8 displays the resulting phase diagram, with a miscibility gap below the $T(x)$ curve, which is symmetric with respect to $x = 1/2$ and which disappears at $x = 1/2$ for $T > T_{max}$. This approximate treatment suggests that $V_{2-2x}Cr_{2x}O_3$, $Ti_{2-2x}Cr_{2x}O_3$ and $Cr_{2-2x}Fe_{2x}O_3$ solid solutions should form in the whole composition range already at ambient temperatures. We note that the present estimation for $Cr_{2-2x}Fe_{2x}O_3$ is in a good agreement with the results of an existing computational study on the mixing thermodynamics in the corundum Fe_2O_3-Cr_2O_3 system[8].

V. CONCLUSION

Within the DFT+U approximation, we have studied a series of mixed $MM'O_3$ compounds (M, M' = Al, Ti, V, Cr, Fe) in three corundum-type structures: ilmenite, $LiNbO_3$, and C. We find that, regardless the precise atomic structure, the local structural and electronic characteristics of most of the compounds are very close to those of their parent corundum M_2O_3 oxides. The two noticeable exceptions are $TiVO_3$ and $TiFeO_3$, for which the structural, electronic, and magnetic characteristics are consistent with a mixing-induced change of the cation oxidation states. We show that this actual oxydo-reduction process can be rationalized by the relative positions of VBM and CBm of the parent oxides, with respect to a common reference. The mixed oxide formation energies that we find are consistent with experimental evidence and, within a mean field approximation, allow to estimate the thermodynamics of mixing of $M_{2-2x}M'_{2x}O_3$ solid solutions at finite temperature. Aside its direct interest for either the considered bulk oxides, or their thin supported films, the present study provides also a reference understanding for a future analysis of low dimensional and/or nano-scale mixed oxide objects. Indeed, the control of the band off-sets of the parent materials by reducing the dimensionality and/or the size of the systems may enable to design and fabricate mixed oxides of required composition and properties.

VI. APPENDIX

TABLE 5. Comparison of the bulk properties of transition metal oxides MO, M_2O_3 and MO_2 in the rocksalt, corundum and rutile structures, obtained with the simulation set-up described in Section II: cation magnetic moment (μ_B) (top) and average M-O bondlength $< d_{M-O} >$ (Å) (bottom) .

μ	MO	M_2O_3	MO_2
Ti	0	0	0
V	2.51	1.75	1.04
Cr	3.71	2.85	2.31
Fe	3.60	4.05	3.62
$< d_{M-O} >$	MO	M_2O_3	MO_2
Ti	2.16	2.06	1.98
V	2.17	2.04	1.93
Cr	2.22	2.02	1.91
Fe	2.19	2.01	1.98

TABLE 6. Same as Table 2 for the $LiNbO_3$ structure. The three shortest range magnetic interactions are given in the following order: in-plane MM', inter-plane MM', inter-plane MM/M'M'.

LiNbO3	$TiAlO_3$	$TiVO_3$	$TiCrO_3$	$TiFeO_3$	$VCrO_3$	$VFeO_3$	$CrFeO_3$
a	5.05	5.09	5.10	5.17	5.04	5.06	5.07
c	13.32	14.12	13.84	13.80	13.98	13.97	13.71
d_{M-O}	2.04;2.11	1.94;2.12	2.00;2.10	1.89;2.14	1.99;2.08	1.97;2.06	2.00;2.03
$d_{M'-O}$	1.88;2.01	2.06;2.10	2.02;2.05	2.08;2.17	1.99;2.06	1.97;2.20	1.96;2.15
Q_M	1.95	2.09	2.00	2.18	1.86	1.92	1.78
$Q_{M'}$	2.49	1.64	1.69	1.43	1.74	1.68	1.74
Q_O	-1.48	-1.24	-1.23	-1.20	-1.20	-1.20	-1.17
μ_M	0.8	0.0	0.7	0.0	1.7	1.6	2.8
$\mu_{M'}$	0	2.2	2.7	3.7	2.9	4.1	4.1
MS	(-,-,AF)	(-,-,AF)	(AF,AF,F)	(-,-,AF)	(AF,F,AF)	(AF,AF,F)	(F,AF,AF)
E^{form}	0.60	-0.33	0.16	-0.73	0.02	-0.01	0.06
Config	$Ti^{3+}Al^{3+}$	$Ti^{4+}V^{2+}$	$Ti^{3+}Cr^{3+}$	$Ti^{4+}Fe^{2+}$	$V^{3+}Cr^{3+}$	$V^{3+}Fe^{3+}$	$Cr^{3+}Fe^{3+}$

[1] T. Fukumura, Z. Jin, A. Ohtomo, H. Koinuma, and M. Kawasaki, Appl. Phys. Lett. **75**, 3366 (1999).
[2] H.-J. Lee, S.-Y. Jeong, C. R. Cho, and C. H. Park, Appl. Phys. Lett. **81**, 4020 (2002).
[3] A.Ohtomo, M. Kawasaki, Y. Sakurai, I. Ohkubo, R. Shiroki, Y. Yoshida, T. Yasuda, Y. Segawa, and H. Koinuma, Mater. Sci. Eng. B **56**, 263 (1998).
[4] M. Radecka, K. Zakrzewska, and M. Rekas, Sensors and Actuators B **47**, 194 (1998).
[5] S. Upadhyay, J. Shrivastava, A. Solanki, S. Choudhary, V. Sharma, P. Kumar, N. Singh, V. R. Satsangi, R. Shrivastav, U. V. Waghmare, and S. Dass, J. Phys. Chem. C **115**, 24373 (2011).
[6] N. L. Allan, G. D. Barrera, M. Y. Lavrentiev, I. T. Todorova, and J. A. Purton, J. Mater. Chem. **11**, 63 (2001).
[7] S. B. Pongsai, J. Mol. Struc.: THEOCHEM **761**, 171 (2006).
[8] S. Benny, R. Grau-Crespo, and N. H. de Leeuw, Phys. Chem. Chem. Phys. **11**, 808 (2009).
[9] F. Maldonado, R. Rivera, and A. Stashans, Physica B **407**, 1262 (2012).
[10] F. Maldonado, C. Novillo, and A. Stashans, Chem. Phys. **393**, 148 (2012).
[11] A. Stashans and S. Jácome, Comput. Mater. Sci. **81**, 353 (2014).
[12] C. D. Valentin and G. Pacchioni, Acc. Chem. Res. **47**, 3233 (2014).
[13] N. Alidoust, M. Lessio, and E. A. Carter, J. Appl. Phys. **119**, 025102 (2016).
[14] T. F. W. Barth and E. Posnjak, Zeitschrift Kristallographie **88**, 265 (1934).
[15] A. Kramer, E. Sutter, D. Su, and M. Batzill, Thin Solid Films **631**, 85 (2017).
[16] G. Kresse and J. Furthmuller, Phys. Rev. B **54**, 11169 (1996).
[17] G. Kresse and J. Hafner, Phys. Rev. B **47**, 558 (1993).
[18] P. E. Blöchl, Phys. Rev. B **50**, 17953 (1994).
[19] G. Kresse and D. Joubert, Phys. Rev. B **59**, 1758 (1999).

TABLE 7. Same as Table 6 for the C structure.

C-structure	$TiAlO_3$	$TiVO_3$	$TiCrO_3$	$TiFeO_3$	$VCrO_3$	$VFeO_3$	$CrFeO_3$
a	5.05	5.07	5.09	5.20	5.05	5.05	5.07
c	13.19	14.20	13.92	13.81	13.96	14.01	13.73
d_{M-O}	2.04;2.10	1.98;2.06	2.02;2.09	1.95;2.05	1.99;2.08	1.96;2.06	1.98;2.06
$d_{M'O}$	1.89;1.98	2.04;2.13	2.00;2.05	2.05;2.28	2.00;2.06	1.99;2.15	1.97;2.11
Q_M	1.90	2.09	1.97	2.19	1.86	1.90	1.77
$Q_{M'}$	2.48	1.65	1.73	1.42	1.75	1.67	1.76
Q_O	-1.46	-1.25	-1.23	-1.20	-1.20	-1.19	-1.18
μ_M	0.0	0.1	0.7	0.0	1.8	1.6	2.8
$\mu_{M'}$	0.	2.2	2.7	3.7	2.9	4.0	4.1
MS	NM	(-,-,AF)	(AF,AF,F)	(-,-,F)	(AF,F,AF)	(AF,AF,F)	(F,AF,AF)
E^{form}	0.40	-0.28	0.19	-0.56	0.04	0.01	0.15
Config	$Ti^{3+}Al^{3+}$	$Ti^{4+}V^{2+}$	$Ti^{3+}Cr^{3+}$	$Ti^{4+}Fe^{2+}$	$V^{3+}Cr^{3+}$	$V^{3+}Fe^{3+}$	$Cr^{3+}Fe^{3+}$

[20] M. Dion, H. Rydberg, E. Schroder, D. C. Langreth, and B. I. Lundqvist, Phys. Rev. Lett. **92**, 246401 (2004).
[21] J. Klimes, D. R. Bowler, and A. Michaelides, J. Phys.: Cond. Matt. **22**, 022201 (2010).
[22] J. Klimes, D. R. Bowler, and A. Michaelides, Phys. Rev. B **83**, 195131 (2011).
[23] V. I. Anisimov, F. Aryasetiawan, and A. I. Liechtenstein, J. Phys.: Condens. Matter **9**, 767 (1997).
[24] S. L. Dudarev, G. A. Botton, S. Y. Savrasov, C. J. Humphreys, and A. P. Sutton, Phys. Rev. B **57**, 1505 (1998).
[25] A. I. Poteryaev, A. I. Lichtenstein, and G. Kotliar, Phys. Rev. Lett. **93**, 086401 (2004).
[26] S. Y. Ezhov, V. I. Anisimov, D. I. Khomskii, and G. A. Sawatzky, Phys. Rev. Lett. **83**, 4136 (1999).
[27] S. Kobayashi, Y. Nohara, S. Yamamoto, and T. Fujiwara, Phys. Rev. B **78**, 155112 (2008).
[28] N. J. Mosey, P. Liao, and E. A. Carter, J. Chem. Phys. **129**, 014103 (2008).
[29] R. F. W. Bader, Chem. Rev. **91**, 983 (1991).
[30] G. Henkelman, A. Arnaldsson, and H. Jonsson, Comput. Mater. Sci. **36**, 354 (2006).
[31] K. Momma and F. Izumi, J. Appl. Crystallogr. **41**, 1272 (2011).
[32] K. Leinenweber, W. Utsumi, Y. Tsuchida, T. Yagi, and K. Kurita, Phys. Chem. Miner. **18**, 244 (1991).
[33] J. Ko and C. T. Prewitt, Phys. Chem. Miner. **15**, 355 (1988).
[34] H. Monkhorst and J. Pack, Phys. Rev. B **13**, 5188 (1976).
[35] WebMineral, http://webmineral.com/ (2014).
[36] C. E. Rice and W. R. Robinson, Acta Crystallogr. B **33**, 1342 (1977).
[37] M. Imada, A. Fujimori, and Y. Tokura, Rev. Mod. Phys. **70**, 1039 (1998).
[38] S.-K. Mo, J. D. Denlinger, H.-D. Kim, J.-H. Park, J. W. Allen, A. Sekiyama, A. Yamasaki, K. Kadono, S. Suga, Y. Saitoh, T. Muro, P. Metcalf, G. Keller, K. Held, V. Eyert, V. I. Anisimov, and D. Vollhardt, Phys. Rev. Lett. **90**, 186403 (2003).
[39] J.-H. Park, L. H. Tjeng, A. Tanaka, J. W. Allen, C. T. Chen, P. Metcalf, J. M. Honig, F. M. F. deGroot, and G. A. Sawatzky, Phys. Rev. B **61**, 11506 (2000).
[40] R. D. Shannon, Acta Crystallogr. A **32**, 751 (1976).
[41] G. Shirane, S. Pickart, and Y. Ishikawa, J. Phys. Soc. Jpn. **14**, 1352 (1959).
[42] N. C. Wilson, J. Muscat, D. Mkhonto, P. E. Ngoepe, and N. M. Harrison, Phys. Rev. B **71**, 075202 (2005).
[43] R. L. Anderson, Solid-State Electron. **5**, 341 (1962).
[44] W. R. Frensley and H. Kroemer, Phys. Rev. B **16**, 2642 (1977).
[45] C. G. Van de Walle and R. M. Martin, Phys. Rev. B **35**, 8154 (1987).
[46] W. A. Harrison, *Electronic Structure and the Properties of Solids* (Freeman, San Francisco, 1980).
[47] S. Massidda, B. I. Min, and A. J. Freeman, Phys. Rev. B **35**, 9871 (1987).
[48] C. Tejedor and F. Flores, J. Phys. C **11**, L19 (1978).
[49] F. Flores and C. Tejedor, J. Phys. C **12**, 731 (1979).
[50] J. Tersoff, Phys. Rev. B **30**, 4874 (1984).
[51] Z. Zhong and P. Hansmann, Phys. Rev. X **7**, 011023 (2017).